Electrochemical Additive Manufacturing Based Design of a Heat Sink for Single Phase Natural Convection Immersion Cooling Application

Conference Paper · November 2023

DOI: 10.1115/IPACK2023-111804

12 authors, including:

Sai Abhideep Pundla
University of Texas at Arlington
6 PUBLICATIONS **1** CITATION
SEE PROFILE

Rohit Suthar
University of Texas at Arlington
6 PUBLICATIONS **2** CITATIONS
SEE PROFILE

Vivek Nair
University of Texas at Arlington
10 PUBLICATIONS **2** CITATIONS
SEE PROFILE

Pratik Bansode
LiquidStack Inc.
44 PUBLICATIONS **257** CITATIONS
SEE PROFILE

Proceedings of the ASME 2023 International Technical Conference and Exhibition on Packaging and Integration of Electronic and Photonic Microsystems
InterPACK2023
October 24-26, 2023, San Diego, California

IPACK2023-111804

ELECTROCHEMICAL ADDITIVE MANUFACTURING BASED DESIGN OF A HEAT SINK FOR SINGLE PHASE NATURAL CONVECTION IMMERSION COOLING APPLICATION

Jacob Lamotte-Dawaghreh
The University of Texas at Arlington
Arlington, TX

Joseph Herring
The University of Texas at Arlington
Arlington, TX

Sai Pundla
The University of Texas at Arlington
Arlington, TX

Rohit Suthar
The University of Texas at Arlington
Arlington, TX

Dr. Vivek Nair
The University of Texas at Arlington
Arlington, TX

Pratik Bansode
The University of Texas at Arlington
Arlington, TX

Gautam Gupta
The University of Texas at Arlington
Arlington, TX

Dr. Dereje Agonafer
The University of Texas at Arlington
Arlington, TX

Joseph Madril
Fabric8Labs
San Diego, CA

Tim Ouradnik
Fabric8Labs
San Diego, CA

Michael Matthews
Fabric8Labs
San Diego, CA

Ian Winfield
Fabric8Labs
San Diego, CA

ABSTRACT

To fulfill the increasing demands of data storage and data processing within modern data centers, a corresponding increase in server performance is necessary. This leads to a subsequent increase in power consumption and heat generation in the servers due to high performance processing units. Currently, air cooling is the most widely used thermal management technique in data centers, but it has started to reach its limitations in cooling of high-power density packaging. Therefore, industries utilizing data centers are looking to single-phase immersion cooling using various dielectric fluids to reduce the operational and cooling costs by enhancing the thermal management of servers. In this study, heat sinks with TPMS lattice structures were designed for application in single-phase immersion cooling of data center servers. These designs are made possible by Electrochemical Additive Manufacturing (ECAM) technology due to their complex topologies. The ECAM process allows for generation of complex heat sink geometries never before possible using traditional manufacturing processes. Geometric complexities including amorphous and porous structures with high surface area to volume ratio enable ECAM heat sinks to have superior heat transfer properties. Our objective is to compare various heat sink geometries by minimizing chip junction temperature in a single-phase immersion cooling setup for natural convection flow regimes. Computational fluid dynamics in ANSYS Fluent is utilized to compare the ECAM heat sink designs. The additively manufactured heat sink designs are evaluated by comparing their thermal performance under natural convection conditions. This study presents a novel approach to heat sink design and bolsters the capability of ECAM-produced heat sinks.

Keywords: single-phase immersion cooling, TPMS, heat sink, ECAM

NOMENCLATURE

$\vec{g}$	Gravity
h	Sensible Enthalpy
k	Thermal Conductivity
k_t	Turbulence Transport Conductivity
p	Pressure
q''	Heat Flux
S_h	Volumetric Heat Generation
T	Temperature
T_0	Operating Temperature
T_{case}	Max Case Temperature
t	Time
$\vec{v}$	Velocity
β	Volumetric Expansion Coefficient
λ	TPMS Porosity
μ	Dynamic Viscosity
ρ	Density
ρ_0	Constant Density

1. INTRODUCTION

Data centers are facilities that are centralized and serve as a location for the storage, distribution, and processing of data through networking and computing equipment that is located remotely. They perform an indispensable function in aiding diverse IT and digital services, encompassing cloud computing,

online applications, and data-intensive operations. Data centers are vital due to their capacity to offer dependable and secure infrastructure for the storage and management of extensive quantities of data. This enables smooth access and processing for individuals, organizations, and businesses.

Global data center electricity use in 2021 was 220-320 TWh [1], or approximately 1.3% of the global electricity demand. Since 2008, heat load per rack has increased rapidly [2]. The total amount of power supplied to the data center is used to power all IT equipment for computing services and to operate a cooling system for removing heat generated by the IT equipment. In addition, data centers utilize electricity for power delivery infrastructures such as UPS and lighting. Figure 1 depicts the division of power consumption in a data center and cooling system. The conventional method of cooling in data centers typically involves the use of air-based cooling systems, such as computer room air conditioning (CRAC) units. These systems use a combination of cool air supply and hot air exhaust to maintain the desired temperature within the data center environment.

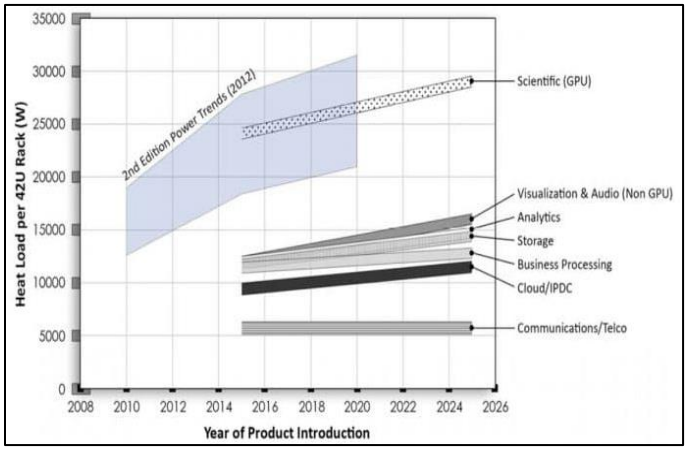

FIGURE 1. POWER CONSUMPTION WITHIN MODERN DATA CENTER

The application of liquid cooling in data centers can be classified into two primary categories based on how the coolant interacts with the electronic components: direct and indirect liquid cooling [3]. In direct cooling, the coolant directly contacts the electronics, whereas indirect liquid cooling involves the use of an intermediary heat exchanger, such as a cold plate, to transfer heat from the processor to the coolant. Indirect liquid cooling includes technologies such as cold plates [4][5], heat pipes, and vapor chambers [6]. Conversely, direct liquid cooling encompasses methods like immersion cooling [7], pool boiling [8], submerged jet impingement [9], and spray cooling, among others. Each of these cooling technologies has limitations in terms of heat transmission, as depicted by the heat transfer coefficient shown in Figure 2. The black bars represent the experimental cooling capacity of the technology studied in literature [10].

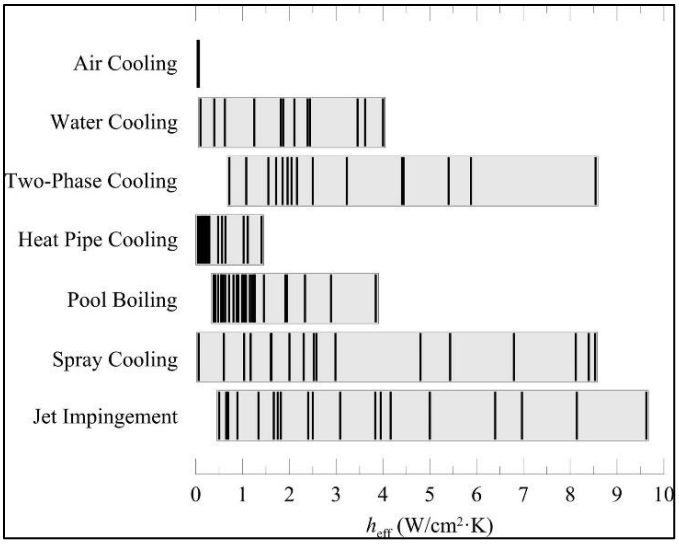

FIGURE 2. COOLING CAPABILITY OF VARIOUS COOLING METHODS [10]

Heat sinks are passive components characterized by their thermal conductivity, which enables the extraction of heat from the CPU. This heat is then dissipated throughout the computer system via fins, which offer a large surface area for effective heat dissipation. By facilitating the transfer of heat from the heat-producing components to the cooling medium, such as air, the temperature of both the processor and the heat sink remains low.

3D printing technologies, also referred to as additive manufacturing (AM) for metal materials, have been recognized as promising techniques for manufacturing heat transfer devices with enhanced performance. Recent studies in literature have demonstrated intriguing examples where the unique characteristics of AM processes are leveraged to optimize well-known heat transfer enhancement techniques. These techniques include the application of AM for producing pin fins, vortex generators, rough surfaces, offset strip fins, and porous media.

Amongst the AM methods, the one that is distinct from the rest is electromechanical additive manufacturing (ECAM). Contrary to most metal AM methods which utilize expensive metal powder feedstocks, ECAM utilizes a water-based feedstock comprised of widely available and low-cost metal salts. The ECAM feedstock is similar to electroplating chemistries which are used in PCB and semiconductor manufacturing. The key innovation which enables the ECAM process is the printhead, a micro-electrode array composed of millions of individually addressable pixels on the scale of 10's of microns. Utilizing this microelectrode array in conjunction with the metal ion rich feedstock, ECAM builds at the atomic level allowing for micron-scale feature resolution, complex internal features, high-purity materials, and rapid scalability to support mass manufacturing.

We have employed the principles of Triply Periodic Minimal Surface (TPMS) structures in the creation of the heat sink designs. TPMS structures belong to a unique category of minimal surfaces that exhibit translational symmetry in three directions [11]. Consequently, TPMS structures consist of infinite, non-self-intersecting, and periodic surface patterns in three primary directions. They are associated with crystallographic space group symmetry [12]. Different lattice structures, such as Gyroid, Schwarz Diamond, and Schwartz Primitive, are based on TPMS. The practical implementation of these structures closely aligns with Metal Additive Manufacturing techniques. These structures not only offer porosity but also enable fluid permeability through their interconnected patterns, while maintaining a higher surface area to volume ratio.

In this study, we compare heat sinks of gyroid sheet lattice structures for a 1U data center server. Baobaid, et. al. showed that under a natural convection flow regime the gyroid sheet TPMS lattice had the best overall performance when compared to the diamond and gyroid solid TPMS lattices [13]. Variables that were studied include the porosity of the lattices, wall thickness, and asymmetry in the unit cell dimensions. We analyzed the impacts of lengthened unit cell dimensions in the flow direction and their results are compared. The lattice heat sink geometries are complex in nature, and their manufacturing is made possible by AM techniques.

2. MODELING PROCEDURE AND DESIGN PARAMETERS

In this study, the lattice-structure heat sink designs were generated using a state-of-the-art software tool, nTopology. This software tool allows for generation of complex lattice structures, including TPMS lattices and general graph unit cell lattices, by way of implicit modeling. The solid domain was modeled within the nTopology platform and exported as an STL file. Figure 3 depicts a gyroid heat sink model that was surface meshed in preparation for STL file export.

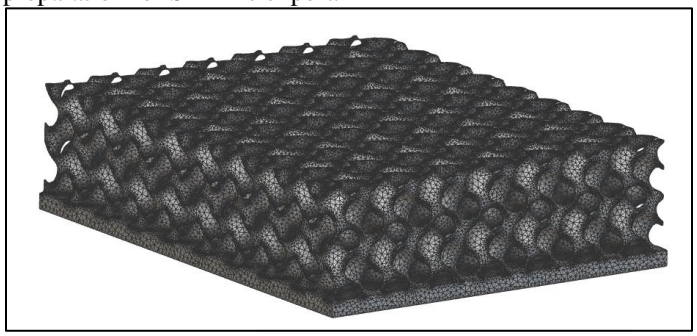

FIGURE 3. GYROID HEAT SINK MODEL WITHIN THE NTOPOLOGY PLATFORM

The STL file was then imported into ANSYS SpaceClaim as faceted geometry, where the boundaries were selected and grouped. Figure 4 below depicts the solid and fluid domains modeled within the SpaceClaim modeler for preprocessing. The SpaceClaim model was then imported into Fluent with Fluent Meshing using the Watertight Meshing (WTM) method. The WTM method produces a conformal mesh at the solid-fluid boundary by using a feature called Share Topology.

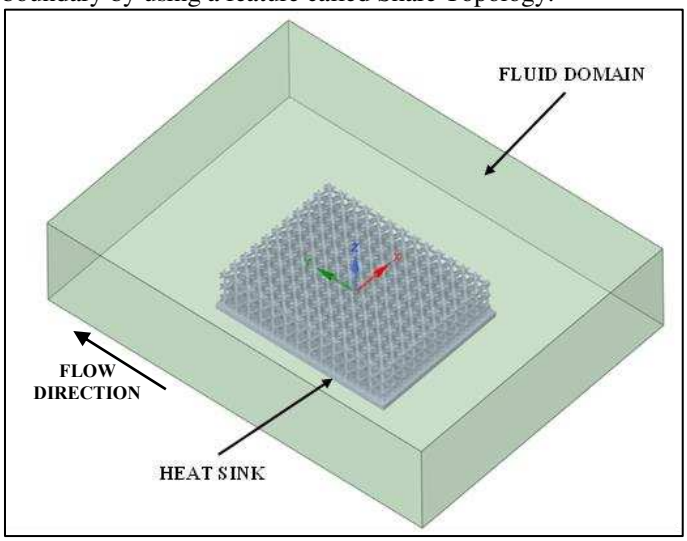

FIGURE 4. PREPROCESSING OF MODEL WITHIN ANSYS SPACECLAIM

The heat sink design parameters were chosen to be representative of a typical 1U data center server CPU heat sink. The 1U server design referenced is the Open Compute Project inspired Wiwynn 1U openEDGE Server [14]. The heat sink design constraints are listed below in Table 1. The heat sink length and width were chosen based on current ECAM print capabilities and print bed size constraints. The heater TDP was chosen to be 250W, which is that of an Intel Xeon Platinum 8450H Processor.

TABLE 1. HEAT SINK DESIGN CONSTRAINTS

Design Constraints	
Base Height	3 mm
Lattice (fin) Height	21 mm
Heat sink Length	90 mm
Heat sink Width	70 mm
Heater TDP	250 W

The various heat sink designs that were chosen to be analyzed are contained within Table 2. Figure 5 portrays the wall thickness and unit cell design parameters on the gyroid heat sink. For the gyroid with asymmetric unit cell sizes, the unit cell dimensions in the flow direction and lattice height were lengthened to resemble more closely a traditional finned heat sink. A heat sink with asymmetric unit cell size is depicted below in Figure 6.

TABLE 2. DESIGN VARIABLES FOR LATTICE HEAT SINKS

Design Variables			
Lattice Type	λ	Wall Thickness	Unit Cell Size
Gyroid TPMS	68%	0.8 mm	5x5x5 mm^3
	85%		10x10x10 mm^3
	68%	1.2 mm	7.3x7.3x7.3 mm^3
	85%		15.2x15.2x15.2 mm^3
Asymmetric Gyroid TPMS	68%	0.8 mm	8x30x30 mm^3
	68%	1.2 mm	14x30x30 mm^3

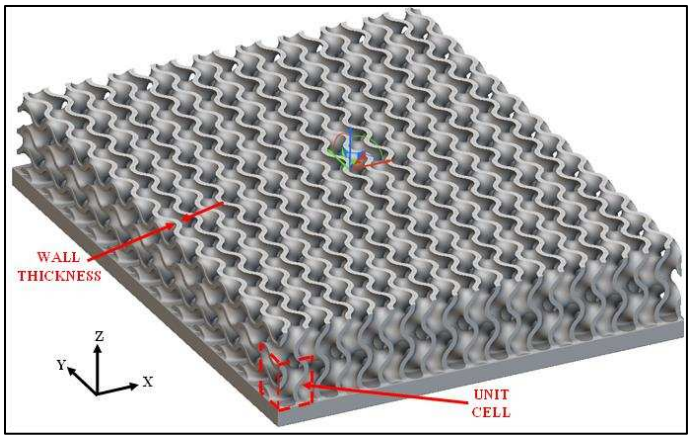

FIGURE 5. DESIGN PARAMETERS FOR TPMS LATTICE HEAT SINK

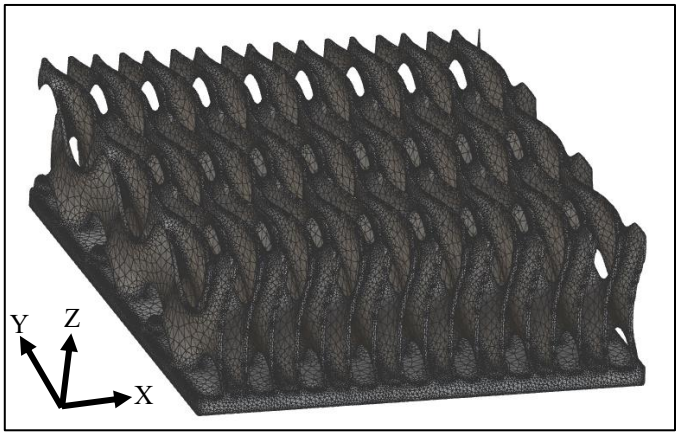

FIGURE 6. GYROID HEAT SINK WITH ASYMMETRIC UNIT CELL SIZE

2.1 Gyroid Lattice Structure

The gyroid sheet TPMS structure that wax analyzed in this study is mathematically defined and has a 3D surface functions that describe the geometry. The mathematical expression that defines a gyroid unit cell is as follows in Equation (1):

$$f(x,y,z) = \cos(x)\sin(y) + \sin(x)\cos(z) + \cos(y)\sin(z) = 0 \quad (1)$$

3. CFD MODEL SETUP

3.1 Boundary Conditions

For the CFD study, the conditions which were chosen to be constant across the analyses are engineered fluid material, inlet fluid temperature, heat sink material, and heat sink design volume. The engineering fluid chosen for this study is ElectroCool 110 (EC-110), which is a commonly used dielectric fluid for immersion cooling applications. The fluid properties of EC-110 defined within the CFD are in accordance with the manufacturer's datasheet [15]. With this working fluid, the inlet temperature was set to be 40°C. The heat sink material chosen is copper; this is, unlike more traditional metallic AM processes, ECAM is capable of printing pure copper, which provides a higher thermal conductivity as compared to other metal alloys.

The CFD model was designed in that there is a solid domain, which is the heat sink, and a fluid domain encompassing that heat sink. The inlet was specified as a velocity inlet with 1e-4 m/s with 40°C inlet temperature. The outlet boundary of the fluid domain was specified as a pressure outlet. The flow direction is in the positive y-direction and gravity is acting in the negative y-direction. This is simply because immersion-cooled data center servers are oriented vertically in the immersion tanks [16]. Figure 7 below depicts the boundary conditions on the fluid domain within the CFD model. Figure 8 depicts the heat flux boundary condition on the heat sink as well as a cross-sectional view of the volume mesh.

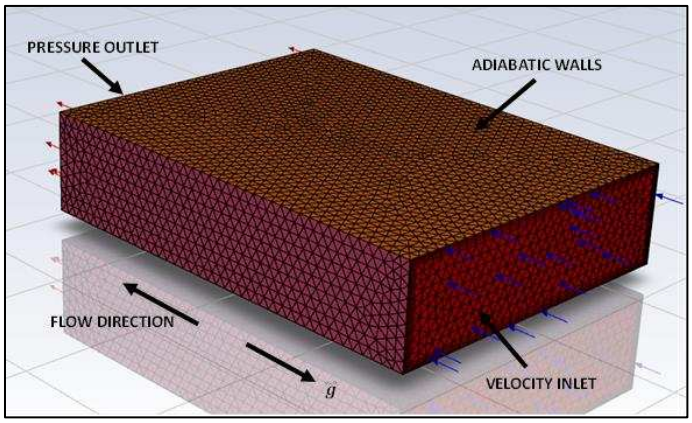

FIGURE 7. BOUNDARY CONDTIONS IN CFD MODEL

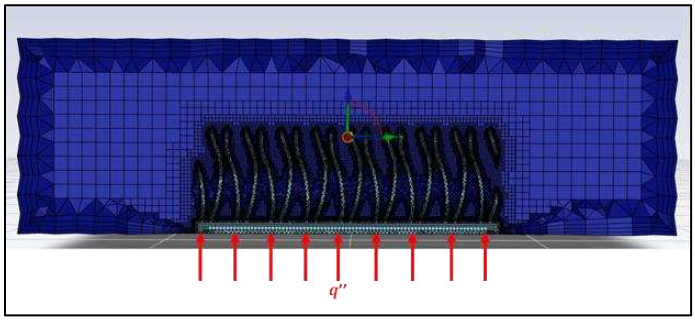

FIGURE 8. HEAT FLUX BOUNDARY CONDITION

3.2 Operating Conditions and CFD Physics

Being that this is a natural convection study, the Boussinesq Model was used. The energy equation was turned on and viscous effects were analyzed using the laminar model. Radiation effects were also considered within the CFD model using Discrete Ordinates (DO). Baobaid et al. showed that under natural convection flow conditions, thermal radiation has significant impacts on the overall heat transfer of gyroid heat sinks. In their study, radiation accounted for approximately 23% of the total heat transfer, and therefore, in this study, we have not considered it to be negligible. The operating density was specified as 820 kg/m^3 based on the material datasheet. The SIMPLE solver was used with the standard under-relaxation factors of 0.3, 1, 1, 0.7, and 1 for the pressure, density, body forces, momentum, and energy solution controls, respectively.

3.3 CFD Model Validation

To validate the CFD model and to ensure convergence, a grid independence study was performed using the gyroid TPMS with 1.2mm wall thickness and 85% porosity. Figure 9 below depicts the max case temperature as a function of the mesh count in the CFD model. It was observed that specifying a grid with edge length of greater than 1/3 of the heat sink wall thickness led to poor results with regards to the model convergence. When the minimum edge length was specified to be at least 1/3 of the heat sink wall thickness, the model converged consistently for minimum grid edge lengths of 1/4 and 1/6 the heat sink wall thickness. Specifying the grid edge length to be 1/3 of the heat sink wall thickness provided results within 1°C, or approximately 1%, of the result when specifying a grid length of 1/6 of the heat sink wall thickness. Since computational burden increases dramatically as minimum grid edge length decreases, it was chosen to specify a minimum grid edge length of 1/3 of that of the heat sink wall thickness for all the CFD simulations.

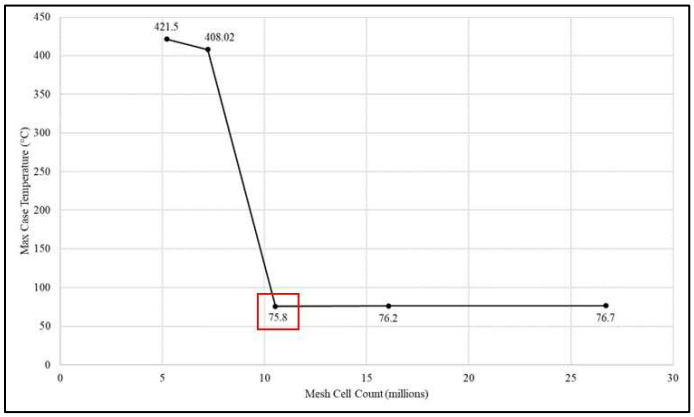

FIGURE 9. GRID INDEPENDENCE OF MAX CASE TEMPERATURE FOR CFD MODEL

4. GOVERNING EQUATIONS FOR NATURAL CONVECTION

For the CFD model, Fluent designates the fluid domain and solid domain and solves the conservation equations for fluid flow. The governing equations (2) through (6) are listed below

Conservation of Mass:

$$\frac{\partial \rho}{\partial t} + \nabla \cdot (\rho \vec{v}) = 0 \tag{2}$$

For incompressible flow, the conservation of mass simplifies to:

$$\nabla \cdot (\vec{v}) = 0 \tag{3}$$

Momentum Equation:

$$\rho \frac{\partial}{\partial t}(\vec{v}) + \rho(\vec{v} \cdot \nabla)\vec{v} = -\nabla p + \rho \vec{g} + \mu \nabla^2 \vec{v} \tag{4}$$

Fluid Domain Energy Equation:

$$\frac{\partial}{\partial t}(\rho h) + \nabla \cdot (\rho h \vec{v}) = -\nabla p + \nabla \cdot [(k + k_t)\nabla T] + S_h \tag{5}$$

Solid Domain Energy Equation:

$$\frac{\partial}{\partial t}(\rho h) = \nabla \cdot (k \nabla T) + S_h \tag{6}$$

The Boussinesq Approximation was used in this CFD model to approximate the density changes, where density differences are only considered in the direction of gravity and ignored elsewhere. The approximation for density is as follows:

$$(\rho - \rho_0)\vec{g} \approx -\rho_0 \beta (T - T_0)\vec{g} \tag{7}$$

5. RESULTS AND DISCUSSION

The gyroid heat sink designs were analyzed with the heat flux applied to the heat sink with the boundary conditions as specified within Section 3.1. The case temperature for each of the designs is listed below in Table 3. Figure 10 shows the comparison between the six designs.

TABLE 3. MAX CASE TEMPERATURE FOR HEAT SINK DESIGNS

Lattice Type	λ	Wall Thickness	T_{case}
Gyroid TPMS	68%	0.8 mm	81.4 °C
	85%		74.1 °C
	68%	1.2 mm	74.0 °C
	85%		75.8 °C
Asymmetric Gyroid TPMS	68%	0.8 mm	75.5 °C
	68%	1.2 mm	80.9 °C

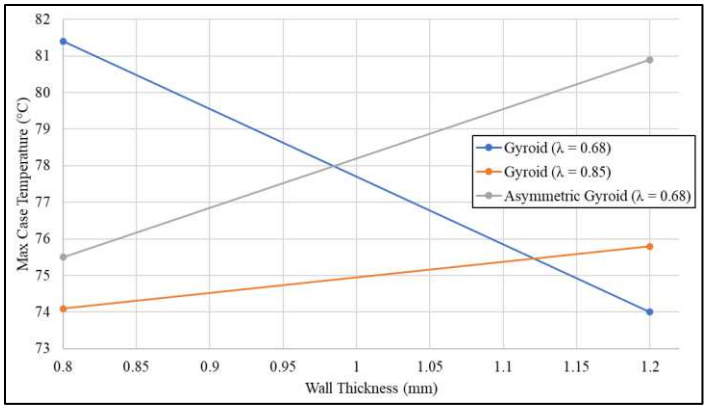

FIGURE 10. MAX CASE TEMPERATURE FOR HEAT SINKS

From the above figure, we see that thermal performance increased as wall thickness increased from 0.8 mm to 1.2 mm for the heat sink with 68% porosity. Meanwhile, the thermal performance decreased for the heat sink with 85% porosity as wall thickness increased. Likewise, the thermal performance decreased in the asymmetric gyroid heat sink with 68% porosity as wall thickness increased.

For the given boundary conditions and in the natural convection flow regime as prescribed, the best performing heat sink is the gyroid TPMS with 1.2 mm wall thickness and 68% porosity. The worst performing design under these conditions is the gyroid TPMS with 0.8 mm wall thickness and 68% porosity. The asymmetric gyroid TPMS performed better with the 0.8 mm wall thickness and performed nearly as poorly as the worst design at 1.2 mm wall thickness. A temperature contour plot for the best performing heat sink in this study is shown in Figure 11 below. Conversely, the temperature contour plot for the worst performing heat sink is shown in Figure 12.

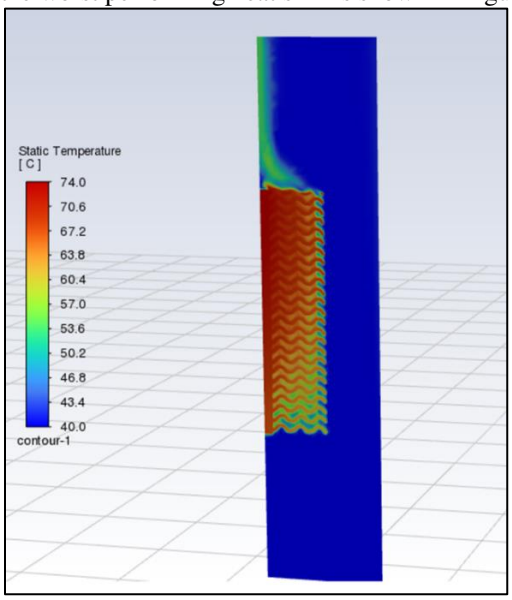

FIGURE 11. TEMPERATURE PLOT FOR BEST PERFORMING HEAT SINK DESIGN

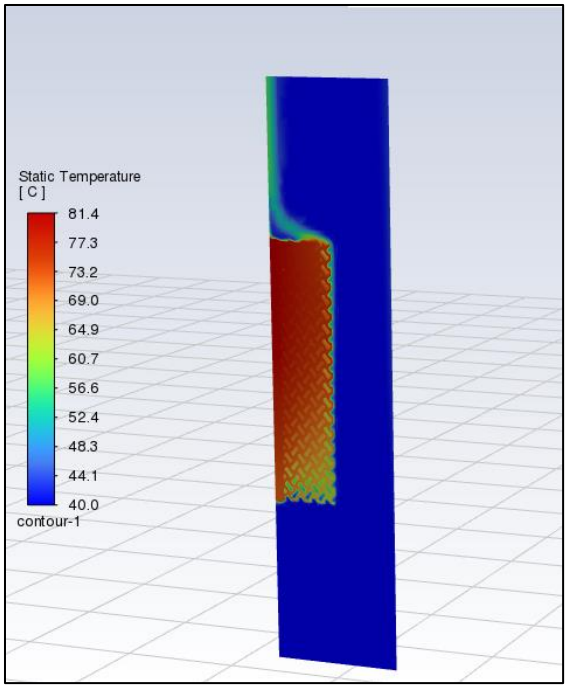

FIGURE 12. TEMPERATURE PLOT FOR WORST PERFORMING HEAT SINK DESIGN

From these temperature results, we believe that the heat sink with the 0.8mm wall thickness and 68% porosity performs worse than the other designs because of restriction in the fluid flow, hindering heat transfer abilities. However, thermal performance for this porosity increases with wall thickness from 0.8mm to 1.2mm, likely due to the presence of additional thermal mass in the heat sink structure, though still restricting flow through the heat sink. Meanwhile, for the heat sink with 85% porosity has increased performance with 0.8mm wall thickness as compared to 1.2mm wall thickness, believed to be caused by allowing the fluid to pass through the heat sink and carry the hot fluid away more easily.

To provide a deeper insight into why the two aforementioned designs are the best and worst, it's necessary to examine the fluid flow profiles through each of the heat sinks. Figures 13 and 14 contain the velocity contour plots through the mid-plane for the best performing heat sink and the worst, respectively. Figures 15 and 16 contain the velocity contour plots across the exit of the heatsink looking into the flow direction.

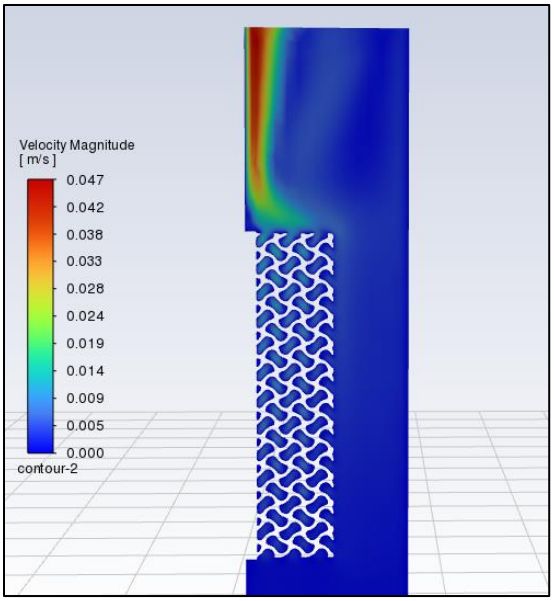

FIGURE 13. MID-PLANE VELOCITY CONTOUR PLOT FOR BEST PERFORMING HEAT SINK DESIGN

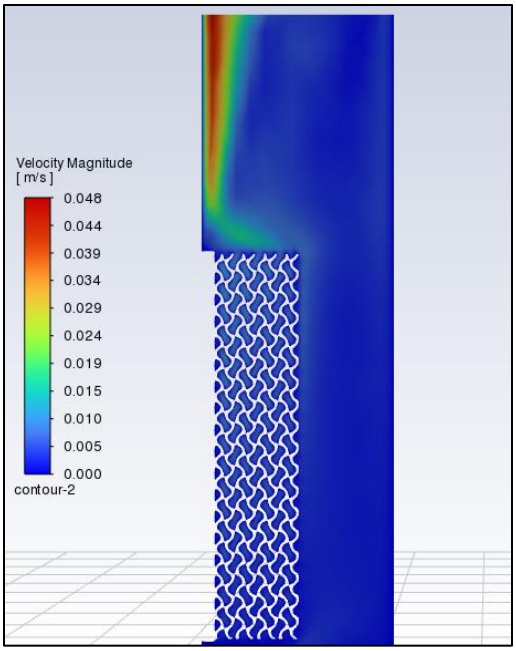

FIGURE 14. MID-PLANE VELOCITY CONTOUR PLOT FOR WORST PERFORMING HEAT SINK DESIGN

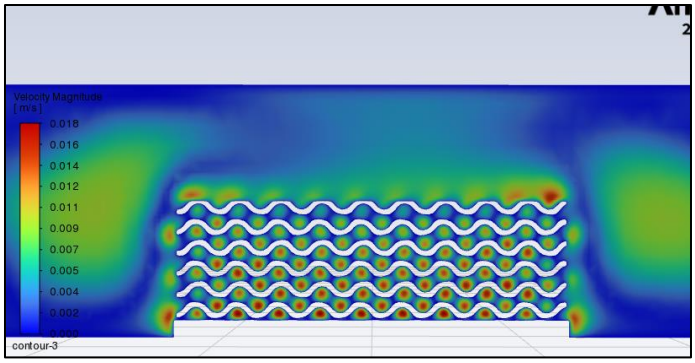

FIGURE 15. VELOCITY CONTOUR PLOT ACROSS EXIT OF BEST PERFOMRING HEAT SINK DESIGN

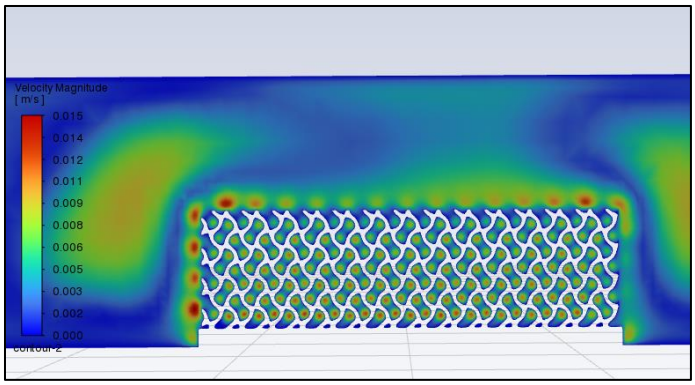

FIGURE 16. VELOCITY CONTOUR PLOT ACROSS EXIT OF BEST PERFOMRING HEAT SINK DESIGN

Examining the velocity profiles of the two designs, it appears that there is restriction in the fluid flow through the length of the heat sink for the worst design. Too much restriction in the flow across the heat sink will hinder its ability to allow fluid to escape after it has been heated. Comparatively, the velocity clearly begins to increase to a greater degree through the length of the heat sink for the better design. Figures 15 and 16 show that the magnitude of velocity exiting the heat sink is considerably greater for the better performing heat sink, which supports the idea of flow restriction leading to worse thermal performance. The flow also has a greater velocity magnitude in different areas, likely based on the local geometry of the heat sink. Comparing the temperature plots reveals a similar trend, where the heat sink temperature rises sooner along the length of the heat sink.

For a heat sink, the goal is to minimize the max case temperature of the component that the heat sink is being used to cool. From Figure 10, we see that minimizing the max case temperature for the 68% porous heat sink may correspond to a wall thickness greater than 1.2mm. Furthermore, for the 85% porous heat sink, minimizing the max case temperature may correspond to a wall thickness less than 0.8mm. In short, we believe that the wall thickness that leads to the minimum point in max case temperature is largely dependent on porosity.

6. CONCLUSIONS

The various lattice heat sink designs were compared, and the results showed that the best overall heat sink was the gyroid TPMS heat sink with 1.2 mm wall thickness and 68% porosity. Moreover, the worst performing heat sink overall was the gyroid TPMS heat sink with 0.8 mm wall thickness and 68% porosity. These heat sink designs, once not so easily producible, are now easily manufacturable by AM processes such as ECAM. Future work with this technology will involve experimental validation and testing of ECAM-produced heat sink designs in single phase immersion cooling applications.

ACKNOWLEDGEMENTS

We would like to acknowledge Fabric8Labs for sponsoring this study. We would also like to acknowledge Yeong-Yan Perng of the ANSYS Fluent team for his contributions in helping to create a functional Fluent workflow for analyzing these complex geometries.

REFERENCES

[1] IEA (2022), Data Centres and Data Transmission Networks, IEA, Paris https://www.iea.org/reports/data-centres-and-data-transmission-networks, License: CC BY 4.0.

[2] ASHRAE. 2018. IT equipment power trends, third edition. Atlanta: ASHRAE.

[3] “Datacenter Cooling Methods | Datacenter cooling best practices,” Submer, Oct. 13, 2015. https://submer.com/blog/datacenter-cooling-methods/

[4] B. Ramakrishnan et al., "Experimental characterization of a cold plate used in warm water cooling of data centers," 2017 33rd Thermal Measurement, Modeling & Management Symposium (SEMI-THERM), San Jose, CA, USA, 2017, pp. 191-196, doi: 10.1109/SEMI-THERM.2017.7896929.

[5] Chen, Gong, Yong Tang, Zhenping Wan, Guisheng Zhong, Heng Tang, and Jian Zeng. "Heat transfer characteristic of an ultra-thin flat plate heat pipe with surface-functional wicks for cooling electronics." *International Communications in Heat and Mass Transfer* 100 (2019): 12-19.

[6] Bulut, Murat, Satish G. Kandlikar, and Nedim Sozbir. "A review of vapor chambers." *Heat Transfer Engineering* 40, no. 19 (2019): 1551-1573.

[7] Shinde, Pravin A., Pratik V. Bansode, Satyam Saini, Rajesh Kasukurthy, Tushar Chauhan, Jimil M. Shah, and Dereje Agonafer. "Experimental analysis for optimization of thermal performance of a server in single phase immersion cooling." In *International Electronic Packaging Technical Conference and Exhibition*, vol. 59322, p. V001T02A014. American Society of Mechanical Engineers, 2019.

[8] Kalani, Ankit, and Satish G. Kandlikar. "Enhanced pool boiling with ethanol at subatmospheric pressures for electronics cooling." Journal of heat transfer 135, no. 11 (2013).

[9] Li, Qiang, Yimin Xuan, and Feng Yu. "Experimental investigation of submerged single jet impingement using Cu–water nanofluid." Applied Thermal Engineering 36 (2012): 426-433.

[10] Kheirabadi, Ali & Groulx, Dominic. (2016). Cooling of Server Electronics: A Design Review of Existing Technology. Applied Thermal Engineering. 105. 10.1016/j.applthermaleng.2016.03.056.

[11] Karcher, Hermann, and Konrad Polthier. "Construction of triply periodic minimal surfaces." Philosophical Transactions of the Royal Society of London. Series A: Mathematical, Physical and Engineering Sciences 354, no. 1715 (1996): 2077-2104.

[12] Hyde, Stephen, Z. Blum, T. Landh, S. Lidin, B. W. Ninham, S. Andersson, and K. Larsson. The language of shape: the role of curvature in condensed matter: physics, chemistry and biology. Elsevier, 1996.

[13] Baobaid, N., Ali, M. I., Khan, K. A., & Abu Al-Rub, R. K. (2022). Fluid flow and heat transfer of porous TPMS architected heat sinks in free convection environment. *Case Studies in Thermal Engineering*, *33*, 101944. https://doi-org.ezproxy.uta.edu/10.1016/j.csite.2022.10194.

[14] N. Wang, “EP100-S1 (Wiwynn 1U openEDGE server)”, Open Compute Project, Revision 0.3, October 30, 2020

[15] Engineered Fluids, “ElectroCool Dielectric Coolants”, EC-ENG-TDS-20200710, July, 2020.

[16] Huang, Y., Ge, J., Chen, Y., & Zhang, C. (2023). Natural and forced convection heat transfer characteristics of single-phase immersion cooling systems for data centers. *International Journal of Heat and Mass Transfer*, *207*. https://doi-org.ezproxy.uta.edu/10.1016/j.ijheatmasstransfer.2023.124023.